Coupled Inductors With Crossed Anisotropy $CoZrTa/SiO_2$ Multilayer Cores

Ryan P. Davies[1,3], Cheng Cheng[2], Noah Sturcken[3], William E. Bailey[2], and Kenneth L. Shepard[1]

[1]Department of Electrical Engineering, Columbia University, New York, NY 10027 USA
[2]Materials Science and Engineering, Department of Applied Physics and Applied Math, Columbia University, New York, NY 10027 USA
[3]Ferric Semiconductor, Inc., New York, NY 10027 USA

Four-turn coupled (flux-closed) inductor structures have been fabricated and tested for use in high-power-density integrated voltage regulator (IVR) applications. Our solenoid-like structure is comprised of a laminated magnetic core of four rungs surrounded by four Cu windings creating four coupled inductors. The magnetic core is made of laminations of ultra-high-vacuum-sputtered [5 nm Ta/200 nm $Co_{91.5}Zr_{4.0}Ta_{4.5}$ (CZT)/7 nm SiO_2] repeated 20 times. Individual CZT layers are deposited under a magnetic bias to induce uniaxial anisotropy. The quad-coupled inductor shows a frequency response with a measured self-inductance of 7.4 nH for one inductor sustained up to 100 MHz and roll-off to half this low-frequency value at ~450 MHz. This inductance is more than 65× higher than what would be calculated from an air-core inductor of equivalent geometry.

***Index Terms*—CoZrTa, laminated magnetic core, magnetic anisotropy, thin film inductor.**

I. Introduction

THE global shift to portable computing has resulted in a concurrent focus on improving the efficiency of power management systems for microprocessor and system-on-chip (SoC) applications. Even as mobile electronic devices continue to add power-depleting features, performance enhancements require increased scalability and a reduction in energy consumption. Integrated voltage regulators (IVRs) offer the potential of scalable power supplies that improve dynamic voltage and frequency scaling for digital integrated circuits [1]. This scalability provides not only more efficient energy consumption, but also allows for the ongoing miniaturization of SoC components. Exploiting package-level air-core inductors, buck-converter IVRs have displayed the most promise with high current densities and efficiencies with a continuous range of conversion ratios [1]–[7]. The use of magnetic-core inductors in these applications and integration of the inductors more tightly with the power train and controller of the converter promises higher efficiencies and support of higher converter densities.

Recent efforts to integrate thin-film magnetic core inductors in the back-end metal stack of existing silicon complementary metal-oxide-semiconductor (CMOS) processes have been pursued to achieve this integration. This work has been primarily based on "yoke-based" thin-film inductors in which the magnetic materials wrap around the windings [1], [8]–[12]. Developing a fabrication process that enables relative compatibility with existing dual Damascene fabrication processes has been one of the challenges in this area. At the same time, alternative solenoid-like inductor topologies have demonstrated up to a 30× increase in inductance compared with air-core inductors of the same geometry [13]. In this paper, we will describe the fabrication of a four-turn solenoid-like coupled inductor topology exploiting electroplating metallization. Through careful design of the laminated magnetic core material and winding topology, we achieve a 65× increase in the inductance over an air-core inductor of the same topology. In Section II, we describe the magnetic material selection. Section III describes the inductor design and fabrication process. Electrical measurements of the resulting structure are presented in Section IV and Section V presents our conclusions.

II. Magnetic Material Selection

$Co_{91.5}Zr_{4.0}Ta_{4.5}$ (CZT) was selected as the magnetic material layer for the inductor core after careful consideration of both Ni-Fe and CZT as candidate metals. Both Ni-Fe and CZT have beneficial soft magnetic properties, including low coercivities and high permeabilities. Thin films of these magnetic materials were sputter deposited in an ultra-high-vacuum (UHV) chamber with a quadruple electromagnet to induce uniaxial anisotropy [14]. Numerous compositional variations of Ni-Fe were investigated, but this material system was deemed unfit for our application due to the inability to induce an anisotropy field (H_k) during deposition that would overcome the shape anisotropy field determined by the dimensions of our magnetic core. CZT, however, allows the induced anisotropy to overcome the shape anisotropy. The deposited amorphous thin films of CZT also have a higher resistivity than those of polycrystalline Ni-Fe [10] allowing for the deposition of thicker magnetic layers before eddy currents became problematic when combined with laminations as described in Section III. The thicker layers also result in higher saturation magnetization levels. Fig. 1 shows easy and hard axes measurements from a B-H loop tracer for our characteristic magnetic layer, 200 nm of CZT, with a coercivity of 0.452 Oe along the hard axis and an H_k of 13.5 Oe.

Manuscript received November 05, 2012; revised December 21, 2012; accepted December 29, 2012. Date of current version July 15, 2013. Corresponding author: R. P. Davies (e-mail: rydavies@gmail.com).

Color versions of one or more of the figures in this paper are available online at http://ieeexplore.ieee.org.

Digital Object Identifier 10.1109/TMAG.2013.2237892

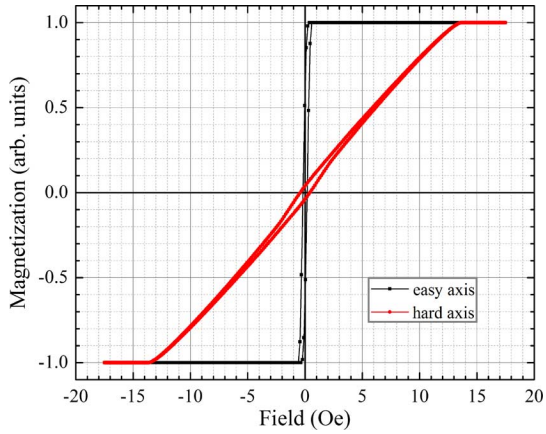

Fig. 1. Magnetization curves for easy and hard axes of a 200 nm CZT film.

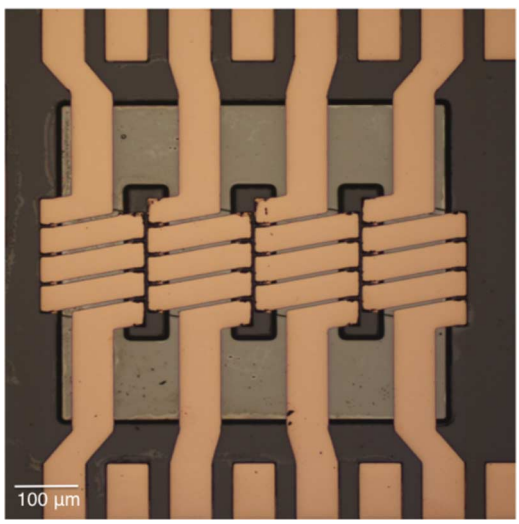

Fig. 2. Top view of a four-turn coupled inductors device. Each rung of the magnetic core ladder forms the core of a solenoid inductor.

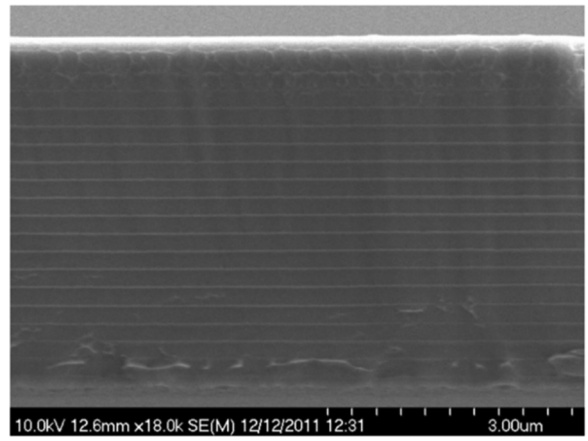

Fig. 3. Cross-sectional SEM image of magnetic core showing 20 repeating laminations of [Ta/CZT/SiO_2] layers. Irregularities in the top and bottom layers are artifacts of the cleaving process.

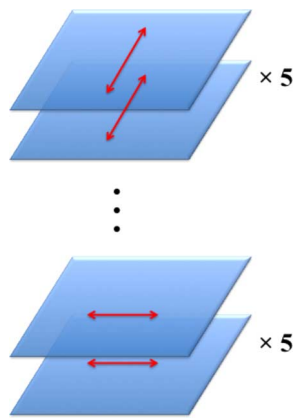

Fig. 4. First ten laminations of [Ta/CZT/SiO_2] are comprised of pairs of adjacent magnetic layers having uniaxial anisotropy (arrows) in one orientation and the next ten layers are comprised of pairs of adjacent magnetic layers having uniaxial anisotropy oriented orthogonal to the previous ten layers.

III. Inductor Design and Fabrication

In addition to the magnetic material selection for the core, inductor design plays an important role in minimizing losses during device operation. Fig. 2 shows the topology of our fabricated four-turn coupled inductors. The device topology is similar to previous work [15], [16] with a core geometry resembling a ladder, where each of the four rungs is the core of a solenoid inductor that is coupled through the stringers of the ladder. Each of the four inductors is inversely coupled with each other; use of this structure allows magnetic saturation of the core to be avoided when operated in a multiphase buck converter [17].

This inductor design optimizes the magnetic and insulating layer thicknesses in the core to avoid the formation of domain walls and eddy currents, which are loss mechanisms at high frequencies. The magnetic core is comprised of 20 repeated laminations of ultra-high-vacuum (UHV)-sputtered [5 nm Ta/200 nm CZT/7 nm SiO_2] layers. Fig. 3 shows a cross-sectional scanning electron microscope (SEM) image of the magnetic core. Individual CZT layers are sputter deposited under a magnetic bias to induce uniaxial anisotropy. Adjacent pairs of CZT layers have similar magnetic anisotropies set using a quadrupole electromagnet during deposition. Five pairs of CZT layers are magnetically biased in one orientation and the following five pairs of CZT layers are biased in the orthogonal orientation as seen in Fig. 4. SiO_2 insulating layers are included to reduce eddy current losses and break exchange coupling between the CZT layers. The SiO_2 thickness is optimized to provide flux closure between adjacent magnetic layers (induced by the easy axis magnetization) without allowing for pinhole formation and the consequential exchange coupling between magnetic layers. Ta layers are used to smooth roughness in the sputtered SiO_2 layers.

The entire inductor fabrication process consists of four distinct layer depositions: three layers to construct the Cu windings and one layer for the magnetic core. The three layers for the Cu windings are fabricated around the magnetic core. We denote the bottom Cu windings layer M1, the Cu via layer as V1, the top Cu windings layer as M2, and the laminated magnetic core as C1. Cu is used for the windings due to its low resistivity and its ability to be planarized in a Damascene process.

The substrate used for the inductor structure is a 1-μm thermally grown SiO_2 layer on Si. The substrate is cleaned and subsequently is subjected to a dehydration bake. To form M1, MicroChem SU-8 photoresist is spun on the substrate, patterned via contact photolithography, developed, and hard baked to create 5-μm deep trenches. Next, a Ta adhesion layer and a Cu seed layer are sputter deposited followed by electrodeposition of $\sim 5.5-\mu$m Cu to overfill the trenches. The electroplated Cu is then planarized in a chemical-mechanical polishing (CMP) tool to remove the Ta and Cu down to the SU-8 and leave 5 μm of Cu in the trenches. Another SU-8 layer is spun on, patterned, and hard baked to provide electrical isolation between the M1 and C1 layers and open up the vias for V1.

Fabrication of the C1 layer proved more difficult due to the multiple material systems present in the laminations of the core. The nonexistence of a wet etch chemistry that effectively removes Ta, CZT, and SiO_2 in a 4- to 5-μm thick stack led to the use of a lift-off process to fabricate C1. The lift-off process consists of spinning on the lift-off resist MicroChem LOR 30B followed by a soft bake. Next, the imaging resist Shipley Microposit S1811 is spun on and soft baked. This bilayer resist stack is patterned and developed to open up the core feature. Due to LOR 30B being dissolved faster than S1811 in the developer, an undercut forms in the lift-off resist. The magnetic core is sputter deposited under a magnetic bias in the system described previously. Due to the limitations of the spin speed and resultant thickness of LOR 30B, the total thickness of the fabricated core cannot exceed $\sim 4.1-\mu$m. The lift-off process is completed by immersing the sample in a solvent to dissolve the LOR 30B and S1811, subsequently causing the unwanted magnetic core material to lift off of the substrate. The undercut in the lift-off resist causes an undesirably sloped sidewall profile along the openings and edges of C1. Investigation into the implication of this sidewall profile on domain formation and orange peel coupling between magnetic layers is ongoing. Future studies will also include utilizing CoO as the insulating layer to allow for an effective wet etch chemistry and minimizing the sidewall profile of the laminated magnetic core.

The V1 and M2 layers are formed by repeating the same steps that were used to fabricate M1, except for the addition of a preclean step before the Ta and Cu sputter deposition steps. In a UHV chamber, the exposed Cu from the M1 and V1 layers are exposed to an Ar glow discharge to remove the native copper oxide. The thickness difference between C1 ($\sim 4.1 - \mu$m) and V1 (5-μm) is purposely incorporated to create an electrical isolation layer of SU-8 between them.

IV. Electrical Measurements

Before taking electrical measurements, a "burn-in" process is performed on the completed four-turn coupled inductors to destroy any copper oxide that remained at the M1/V1 and V1/M2 interfaces. A native copper oxide layer forms at these junctions when the Cu windings are exposed to ambient atmosphere before the adhesion and seed layer depositions. Unfortunately, the Ar plasma etch employed before these depositions is not completely effective in removing this oxide. For the process, a voltage of 10 V is applied across the Cu windings of each inductor with a current limit of 0.5 A for 5 minutes. A significant reduction in resistance is typically observed within the first two minutes, after which the coil resistance stabilizes.

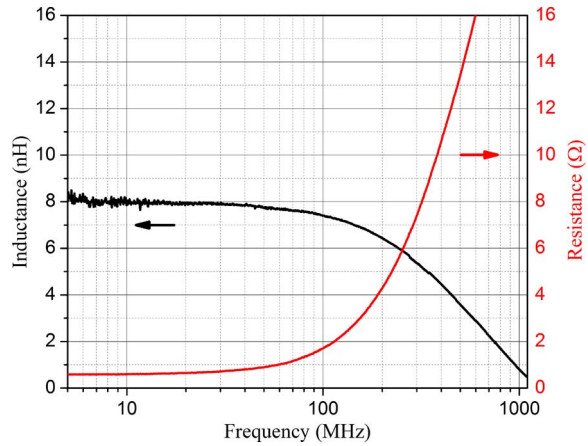

Fig. 5. Frequency response of inductance and resistance for a single solenoid inductor.

DC measurements of the inductors are taken with a set of DC probes and an Agilent 4155C Parameter Analyzer. Four port AC measurements are taken with a pair of Cacade Microtech Dual Infinity Probes (GSGSG -100 μm), and Agilent N5230A four-port network analyzer, which operates from 300 kHz to 20 GHz. Measured scattering parameters are converted to admittance parameters and then fitted to a circuit network of the inductors that includes series resistance, mutual, and leakage inductance.

Electrical measurements showed a DC resistance for the 5-μm thick Cu windings of $\sim 0.48\ \Omega$, which is $4\times$ higher than the expected value of $0.12\ \Omega$. The higher resistance is attributed to the copper oxide at the M1/V1 and V1/M2 interfaces that remains after the "burn-in" process described above. Fig. 5 shows the frequency response of the inductance and resistance for a single inductor with a measured self-inductance of 7.4 nH sustained up to 100 MHz and roll-off to half this low-frequency value at $\sim$450 MHz. This measured inductance is more than $65\times$ higher than what would be calculated from an air-core inductor of equivalent geometry and results in an inductance density of 82 $\mathrm{nH/mm^2}$ for our inductor dimensions.

V. Discussion

The inductors have been simulated in the finite-element analysis solver, Maxwell, and simulations show low frequency inductance, coupling coefficient, and resistance values of 8.25 nH, $\sim$0.262, and $0.124\ \Omega$, respectively. When the simulated magnetic core is modified to have uniaxial anisotropy with hard axis oriented along the center of each coil, the low frequency inductance, coupling coefficient, and resistance values are 5.88 nH, $\sim$0.1765, and $0.124\ \Omega$, respectively. The measured coupling coefficient is only 0.015, with the discrepancy between simulated and measured coupling coefficients likely due to domain wall pinning in the stringers of the magnetic core. This pinning reduces the permeability in this section of the core, and consequently, the coupling between inductors. An improved inductor design and fabrication process is being developed to prevent

domain wall pinning, which should consequently improve coupling.

Extending the analysis developed in Herget *et al.* [18] to four phases, these inductors would achieve a peak effective efficiency of ∼86% while operating in a buck converter with switching frequency of 200 MHz, and would have a saturation current of 18 mA, corresponding to a current density of $\sim\ 0.19\ \mathrm{A/mm^2}$. However, improved magnetic material processing should improve the coupling between inductors, increasing the coupling coefficient to the simulated value of ∼0.262, which would elevated the effective efficiency to 90% and current density to 3.0 $\mathrm{A/mm^2}$.

VI. Conclusion

Four-turn coupled inductors comprised of Cu windings surrounding rungs of a laminated magnetic core have been fabricated to determine their effectiveness for power electronic applications. The laminated core was composed of repeated layers of Ta, CZT, and $\mathrm{SiO_2}$. CZT was chosen as the magnetic layer in the core due to its low coercivity, high permeability, and high resistivity as a result of its amorphous structure. Due to limitations imposed by fabrication challenges and low yields, only single inductor measurements were performed. An inductance of 7.4 nH and an inductance density of 82 $\mathrm{nH/mm^2}$ were measured for a single inductor up to 100 MHz, displaying a frequency response suitable for high-power-density IVR applications. Modifications to the inductor design and fabrication process are ongoing to improve the yield and quality of the inductors.

Acknowledgment

This work was supported in part by the U.S. Department of Energy (DE-EE0002892) and the National Science Foundation (EECS-0903466).

References

[1] N. Sturcken *et al.*, "A 2.5D integrated voltage regulator using coupled-magnetic-core inductors on silicon interposer delivering 10.8 $\mathrm{A/mm^2}$," in *Proc. IEEE Int. Solid-State Circuits Conf. (ISSCC)*, 2012, pp. 400–401.

[2] G. Schrom *et al.*, "A 480-MHz, multi-phase interleaved buck DC-DC converter with hysteretic control," in *Proc. IEEE 35th Annu. Power Electron. Specialists Conf. (PESC)*, 2004, vol. 6, pp. 4702–4707.

[3] P. Hazucha *et al.*, "A 233-MHz 80%–87% efficient four-phase DC-DC converter utilizing air-core inductors on package," *IEEE J. Solid-State Circuits*, vol. 40, no. 4, pp. 838–845, Apr. 2005.

[4] G. Schrom *et al.*, "A 100 MHz eight-phase buck converter delivering 12 A in 25 $\mathrm{mm^2}$ using air-core inductors," in *Proc. 22nd Annu. IEEE Appl. Power Electron. Conf. (APEC) 2007,* , 2007, pp. 727–730.

[5] G. Schrom, F. Paillet, and J. Hahn, "A 60 MHz 50 W fine-grain package integrated VR powering a CPU from 3.3 V," presented at the Appl. Power Electron. Conf. (APEC)—Special Presentation, 2010.

[6] N. Sturcken, M. Petracca, S. Warren, L. P. Carloni, A. V. Peterchev, and K. L. Shepard, "An integrated four-phase buck converter delivering 1 $\mathrm{A/mm^2}$ with 700 ps controller delay and network-on-chip load in 45-nm SOI," in *Proc. 2011 IEEE Custom Integr. Circuits Conf. (CICC)*, 2011, pp. 1–4, 19–21.

[7] J. T. DiBene *et al.*, "A 400 Amp fully Integrated silicon voltage regulator with in-die magnetically coupled embedded inductors," presented at the Appl. Power Electron. Conf. (APEC)—Special Presentation, 2010.

[8] D. S. Gardner, G. Schrom, P. Hazucha, F. Paillet, T. Karnik, and S. Borkar, "Integrated on-chip inductors with magnetic films," *IEEE Trans. Magn.*, vol. 43, no. 6, pp. 2615–2617, Jun. 2007.

[9] D. S. Gardner, G. Schrom, P. Hazucha, and F. Paillet, "Integrated on-chip inductors using magnetic material (invited)," *J. Appl. Phys.*, vol. 103, p. 07E927, 2008.

[10] D. S. Gardner, G. Schrom, F. Paillet, B. Jamieson, T. Karnik, and S. Borkar, "Review of on-chip inductor structures with magnetic films," *IEEE Trans. Magn.*, vol. 45, no. 10, pp. 4760–4766, Oct. 2009.

[11] W. Xu *et al.*, "Sub-100 $\mu\mathrm{m}$ scale on-chip inductors with CoZrTa for GHz applications," *J. Appl. Phys.*, vol. 109, p. 07A316, 2011.

[12] N. Wang *et al.*, "Integrated on-chip inductors with electroplated magnetic yokes (invited)," *J. Appl. Phys.*, vol. 111, no. 7, p. 07E732, 2012.

[13] D. W. Lee, K.-P. Hwang, and S. X. Wang, "Fabrication and analysis of high-performance integrated solenoid inductor with magnetic core," *IEEE Trans. Magn*, vol. 44, no. 11, pp. 4089–4095, Nov. 2008.

[14] C. Cheng, N. Sturcken, K. Shepard, and W. E. Bailey, "Vector control of induced magnetic anisotropy using an *in-situ* quadrupole electromagnet in ultrahigh vacuum sputtering," *Rev. Sci. Instrum.*, vol. 83, p. 063903, 2012.

[15] P.-L. Wong, P. Xu, P. Yang, and F. C. Lee, "Performance improvements of interleaving VRMs with coupling inductors," *IEEE Trans. Power Electron.*, vol. 16, no. 4, pp. 499–507, Apr. 2001.

[16] J. Li, C. R. Sullivan, and A. Schultz, "Coupled-inductor design optimization for fast-response low-voltage DC-DC converters," in *Proc. 27th Annu. IEEE Appl. Power Electron. Conf. (APEC)*, 2002, vol. 2, pp. 817–823.

[17] N. Sturcken, R. Davies, C. Cheng, W. E. Bailey, and K. L. Shepard, "Design of coupled power inductors with crossed anisotropy magnetic core for integrated power conversion," in *Proc. 27th Annu. IEEE Appl. Power Electron. Conf. (APEC)*, 2012, pp. 417–423.

[18] P. Herget *et al.*, "A study of current density limits due to saturation in thin film magnetic inductors for on-chip power conversion," *IEEE Trans. Magn.*, vol. 48, no. 11, pp. 4119–4122, Nov. 2012.